

RADIO OBSERVATIONS OF SN 2004dk WITH VLITE CONFIRM LATE-TIME RE-BRIGHTENING

A. BALASUBRAMANIAN^{1,*}, A. CORSI¹, E. POLISENSKY², T. E. CLARKE², N. E. KASSIM²

Draft version June 23, 2021

ABSTRACT

The study of stripped-envelope core-collapse supernovae (SNe), with evidence for strong interaction of SN ejecta with the circumstellar medium (CSM), provides insights into the pre-supernova progenitor, and a fast-forwarded view of the progenitor mass-loss history. In this context, we present late-time radio observations of SN 2004dk, a type Ibc supernova located in the galaxy, NGC 6118, at a distance of $d_L \approx 23$ Mpc. About 15 years after explosion, SN 2004dk has shown evidence for H α emission, possibly linked to the SN ejecta interacting with an H-rich CSM. Using data from the VLA Low Band Ionosphere and Transient Experiment (VLITE), we confirm the presence of a late-time radio re-brightening accompanying the observed H α emission. We model the SN 2004dk radio light curves within the (spherically symmetric) synchrotron-self-absorption (SSA) model. Within this model, our VLITE observations combined with previously collected VLA data favor an interpretation of SN 2004dk as a strongly CSM-interacting radio SN going through a complex environment shaped by a non-steady mass-loss from the SN progenitor.

Subject headings: supernovae: general – supernovae: individual (SN2004dk) – radiation mechanisms: general – radio continuum: general

1. INTRODUCTION

Type Ibc supernovae (SNe) are a class of massive star core-collapse explosions that lack Hydrogen (H) features in their spectra and are thus referred to as stripped-envelope core-collapse SNe. They account for $\approx 25\%$ of the local core-collapse SN population (Smith et al. 2011). The presence or absence of Helium (He) features allows for further classification of these core-collapse explosions into SNe of type Ib (He-rich) and type Ic (He-poor) (see e.g., Filippenko 1997). The physical processes that drive mass loss in evolved massive stars that constitute the pre-SN progenitors, as well as the physics of the pre-supernova progenitors themselves, are yet to be understood. Several models have been proposed which include ejection of envelopes of massive Wolf-Rayet (WR) stars through strong dense winds (Begelman & Sarazin 1986; Woosley et al. 1995), or accretion from a nearby companion which strips the massive star of its H-rich layer (Wheeler & Levreault 1985; Podsiadlowski et al. 1992).

Studying the properties of the circumstellar medium (CSM) of Ibc SNe is crucial to shed light on the physics of mass loss, and can provide valuable clues on the pre-SN progenitor. Following the collapse of the core, a shock wave travels outwards and reaches the outer envelopes of the star. The emission in X-rays (as well as UV and light at blue visible wavelengths) that accompanies the so-called shock breakout, can help constrain the progenitor radius (Piro & Nakar 2013; Ho et al. 2019). Subsequently, the shock front begins interacting with matter ejected by the pre-SN progenitor. Radio (and X-ray) observations can be used to probe this interaction, providing information on the mass loss history of the stellar progenitor before its SN explosion (e.g., Soderberg et al.

2005, 2006; Corsi et al. 2014; Margutti et al. 2017; Rivera Sandoval et al. 2018; Palliyaguru et al. 2019).

In this paper we report on the late-time radio observations of SN 2004dk, a Type Ib SN characterized by radio emission with a late-time re-brightening. About 10 years after explosion, SN 2004dk has shown evidence of H α emission likely linked to the SN ejecta interacting with an H-rich CSM (Pooley et al. 2019). X-ray emission associated with SN 2004dk was detected between about 10 days and 14.5 years since explosion (Pooley 2007; Pooley et al. 2019). Radio monitoring at GHz frequencies up to about 4.5 years since explosion revealed a GHz flux that initially decayed with time, followed by a re-brightening (see Stockdale et al. 2009; Wellons et al. 2012). The early-time radio light curve evolution agreed with a synchrotron self-absorbed (SSA) model where the SN shock propagates into a steady-state wind with a density profile scaling as $\rho \propto r^{-2}$ (Chevalier & Fransson 2006). The radio re-brightening observed around 4.5 yrs since explosion was interpreted also within the SSA model, and attributed to the collision of the forward shock with a denser CSM (see Stockdale et al. 2009; Wellons et al. 2012). More recently, Pooley et al. (2019) have analyzed the late-time optical and X-ray observations of SN 2004dk in the “wind bubble model”, where the late-time emission results from the SN shock interaction with a complex CSM that has been previously structured by interacting fast and slow winds.

Here, we present new radio observations of SN 2004dk carried out about 14 years after explosion with the VLA Low Band Ionosphere and Transient Experiment (VLITE¹; Clarke et al. 2016). SN 2004dk is the first SN of its type to be detected with VLITE. Low-frequency radio observations are critical to constrain the absorption mechanisms and the CSM structure. We thus re-analyze the radio dataset of SN 2004dk within the SSA model including our low-frequency observations.

¹ Department of Physics and Astronomy, Texas Tech University, Box 1051, Lubbock, TX 79409-1051, USA

² Naval Research Laboratory, Code 7213, 4555 Overlook Avenue, SW, Washington, DC 20375, USA

* Email : arvind.balasubramanian@ttu.edu

¹ <https://www.nrl.navy.mil/rsd/7210/7213/vlite>

Our paper is organized as follows. In Section 2, we summarize previous observations of SN2004dk that are relevant for this study, present our VLITE observations and briefly describe the data reduction process. In Section 3, we describe the SSA model used for our analysis. In Section 4, we present the results of our light curve fits for SN2004dk. In Section 5, we discuss our results and conclude.

2. OBSERVATIONS AND DATA REDUCTION

SN 2004dk was discovered by the the Katzman Automatic Imaging Telescope (KAIT) on 2004 August 1.19 UT (thus, hereafter we assume an explosion time of $t_e = 2453217.69$ JD (J2000), 2 days before August 1.19 (see [Graham & Li 2004a](#))) at RA=16h21m48.87s, Dec=-02d16m17.6s. SN 2004dk is located in the galaxy, NGC 6118, at a distance of ≈ 23 Mpc ([Graham & Li 2004b](#)). Subsequent spectroscopic observations helped classify this SN as a He-rich, H-poor, Type Ib ([Filippenko et al. 2004](#)). SN 2004dk was also detected in X-rays starting from about 10 days since optical discovery ([Pooley 2007](#)).

2.1. VLA observations

SN 2004dk was first observed at GHz radio frequencies at about 8 days after explosion, with the Karl G. Jansky Very Large Array (VLA). Follow-up observations with the VLA continued until 2009 ($\Delta t \sim 1912$ days since explosion; [Wellons et al. 2012](#); [Stockdale et al. 2009](#)). A summary of the radio observations carried out with the VLA between 4.9 GHz and 22.5 GHz is reported in the first section of Table 1 (adapted from [Wellons et al. 2012](#)). The 8.5 GHz light curve of SN 2004dk peaks at ~ 14 days from the SN explosion with a flux density $F_\nu \approx 2.5$ mJy. At an epoch of $\Delta t \sim 1700$ days since explosion, a re-brightening is observed at 4.9 GHz and 8.5 GHz. Late-time optical observations show evidence for broad H α emission, suggesting that the re-brightening observed at ~ 1700 days can be attributed to the interaction of the SN ejecta with the previously ejected H-envelope by the progenitor ([Vinko et al. 2017](#); [Mauerhan et al. 2018](#)).

A more recent GHz radio observation of the SN 2004dk field was carried out on 2018 April 7.4 UT ($\Delta t \sim 5000$ days since explosion) with the VLA in its A configuration (VLA/18A-119, PI: Margutti; see Table 1). 3C286 was used as flux calibrator and J1557-0001 was used as complex gain calibrator. We calibrated this data in CASA ([McMullin et al. 2007](#)) using the standard VLA calibration pipeline, and then manually inspected and flagged the calibrated data for Radio Frequency Interference (RFI). After imaging the field with the `clean` task interactively, we used the CASA task `imfit` to obtain the integrated flux density of SN 2004dk (and the associated statistical error) within a circular region of radius $0.33''$ (nominal VLA resolution at the observed frequency for A-array configuration) centered on the optical position of the SN. A 5% absolute flux calibration error was added in quadrature to the flux density error returned by `imfit` (e.g., [Ofek et al. 2011](#)).

2.2. VLITE observations

VLITE is a commensal, low-frequency system on the VLA that runs in parallel (since 2014) with nearly all observations above 1 GHz. VLITE provides real-time correlation of the signal from a subset of VLA antennas

using the low-band receiver system ([Clarke et al. 2011](#)) and a dedicated DiFX-based software correlator ([Deller et al. 2007](#)). The VLITE system processes 64 MHz of bandwidth centered on 352 MHz, but due to strong RFI in the upper portion of the band, the usable frequency range is limited to an RFI-free band of ~ 40 MHz, centered on 338 MHz.

SN 2004dk was observed by VLITE on 2018 April 7, 2019 August 30, 2020 December 28 and 2021 January 1 UT. These dates correspond to $\Delta t \sim 5000, 5500$ and 6000 days after the SN 2004dk explosion, respectively. The VLITE data are reported in the bottom section of Table 1. SN 2004dk is the first SN to be detected at sub-GHz frequencies by VLITE. VLITE data were processed using a dedicated calibration pipeline based on a combination of `Obit` ([Cotton 2008](#)) and AIPS ([van Moorsel et al. 1996](#)) data reduction packages. The calibration pipeline uses standard automated tasks for the removal of RFI and follows common techniques of radio-interferometric data reduction, including delay, gain, and bandpass calibration (for details on the pipeline data reduction see [Polisensky et al. \(2016\)](#)). The flux density scale is set using [Perley & Butler \(2017\)](#). The final VLITE images have restoring beams of approximately $6'' \times 4''$ and rms noise $0.5 - 1$ mJy beam $^{-1}$ (1σ). Flux densities were measured with PyBDSF ([Mohan & Rafferty 2015](#)) via the VLITE Database Pipeline ([Polisensky et al. 2019](#)). We conservatively adopt 20% flux density errors that include local image noise as well as fitting and flux-scale uncertainties.

2.3. VLASS archival observation

The VLA Sky Survey (VLASS) is an ongoing 2–4 GHz survey of the entire sky visible to the VLA i.e., $\delta > -40$ deg for a total of about 33,885 deg 2 of the sky ([Lacy et al. 2020](#)).

We queried the VLASS quick look image archive for fields centered at < 1 deg from the optical position of SN 2004dk. We manually inspected the retrieved VLASS images and identified a source coincident with the optical position of SN 2004dk. The VLASS field containing the SN (observed in epoch 1.2 2) was then analyzed using the CASA task `imfit` to obtain the integrated source flux density (and corresponding statistical error), using a circular region of radius $2.5''$ (nominal VLASS resolution) centered at the optical SN position. In order to account for absolute flux calibration errors, we added in quadrature to the integrated flux error returned by `imfit` a fractional 10% error (as VLASS Epoch 1 total flux densities are estimated to have systematic errors of order 10% 2). Our results are reported in the bottom section of Table 1, and Figure 1 (center and right panels) shows the VLASS radio contours of SN 2004dk.

3. RADIO LIGHT CURVE MODELLING

The SSA model ([Chevalier 1998](#); [Chevalier & Fransson 2006](#)) has been used successfully to describe late-time radio emission powered by SN ejecta-CSM interaction (e.g., [Soderberg et al. 2005](#); [Wellons et al. 2012](#); [Palliyaguru & Corsi 2019](#); [Palliyaguru et al. 2019](#)). Within the SSA model, for a smooth CSM profile such as the one

² <https://science.nrao.edu/science/surveys/vlass/vlass-epoch-1-quick-look-users-guide>

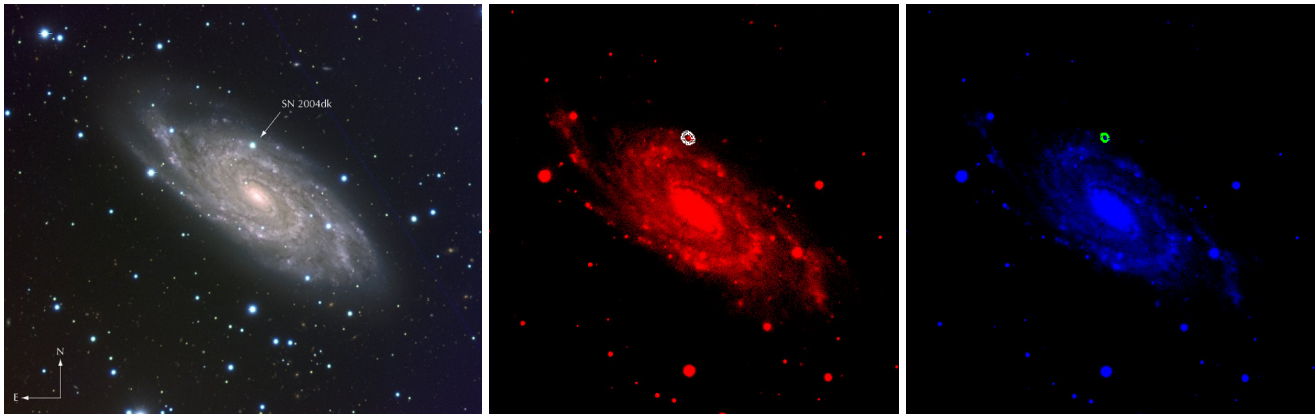


FIG. 1.— *Left*: VLT MELIPAL+VIMOS image (www.eso.org/public/images/eso0436b/) of the spiral galaxy NGC 6118 and SN 2004dk. *Center*: Radio contours observed using VLITE (white - 10σ outermost contour, see Table 1 for the data) on 01 Jan 2021 UT and *Right*: VLASS (green - 7σ outermost contour, see Table 1 for the data), both overlotted on an r-band Pan-STARRS1 image of the field (Flewelling et al. 2020) with the help of SAOImageDS9 (Joye & Mandel 2003).

predicted to arise from a constant mass-loss rate, constant velocity pre-SN wind, the observed radio emission is characterized by a smooth turn-on first at higher frequencies, and later at lower frequencies. This evolution can be explained as a consequence of a self-absorption frequency which decreases with time as the SN shock propagates toward lower density regions. Modifications to this scenario include an initial exponential rise of the low-frequency radio flux due to free-free absorption in the ionized CSM (an effect usually relevant at early

times; see e.g. Weiler et al. 1990; Chevalier 1998), as well as flux variations associated with a non-smooth CSM profile, perhaps associated with eruptive mass-loss from the SN progenitor (Wellons et al. 2012; Palliyaguru & Corsi 2019; Corsi et al. 2014; Palliyaguru et al. 2019). A detailed description of the SSA model focused on its application to radio SNe can be found in Soderberg et al. (2005). In what follows, we summarize briefly the model so as to introduce notation relevant for our analysis of the SN 2004dk data.

TABLE 1 Radio measurements of SN2004dk flux density until Aug 2019. Data until Oct 2009 UT are from Wellons et al. (2012). The last four rows contain the more recent VLITE and VLA observations presented for the first time in this paper.

Date (UT)	Epoch (days)	340 MHz (mJy)	3.0 GHz (mJy)	4.9 GHz (mJy)	6.0 GHz (mJy)	8.5 GHz (mJy)	15.0 GHz (mJy)	22.5 GHz (mJy)	Inst.
2004 Aug 7.1	7.9	1.30 ± 0.05	VLA-D
2004 Aug 11.0	11.8	0.87 ± 0.06	...	2.11 ± 0.06	...	2.78 ± 0.33	VLA-D
2004 Aug 13.0	13.8	1.09 ± 0.06	...	2.42 ± 0.06	3.57 ± 0.26	2.72 ± 0.37	VLA-D
2004 Sep 2.0	33.8	1.80 ± 0.09	...	1.56 ± 0.13	0.79 ± 0.21	0.69 ± 0.18	VLA-D
2004 Sep 10.0	41.8	1.06 ± 0.07	...	0.81 ± 0.15	...	<0.43	VLA-A
2004 Sep 18.0	49.8	0.86 ± 0.10	...	1.19 ± 0.11	...	<0.47	VLA-A
2004 Oct 4.1	65.9	0.46 ± 0.15	...	0.41 ± 0.09	<0.34	<1.41	VLA-A
2004 Oct 17.8	79.6	0.56 ± 0.10	...	0.47 ± 0.12	<0.92	...	VLA-A
2005 Feb 12.4	197.2	<0.26	...	<0.17	VLA-BnA
2009 Feb 12.6	1658.4	0.22 ± 0.06	VLA-B
2009 Feb 24.5	1670.3	0.21 ± 0.03	...	0.19 ± 0.03	VLA-B
2009 Apr 2.6	1707.4	0.34 ± 0.07	...	<0.08	VLA-B
2009 Apr 19.0	1723.8	0.21 ± 0.02	...	0.15 ± 0.02	VLA-C
2009 Sep 19.8	1877.6	0.28 ± 0.05	...	0.17 ± 0.02	...	<0.57	VLA-B
2009 Oct 26.8	1914.6	<0.27	VLA-D
2018 Apr 7.4	4999.2	17.10 ± 3.42	VLITE
2018 Apr 7.4	4999.2	4.06 ± 0.24^a	VLA-A
2019 May 20.4	5407.2	...	6.46 ± 0.65^b	VLASS
2019 Aug 30.0	5508.8	11.20 ± 2.24	VLITE
2020 Dec 27.7	5994.5	21.53 ± 4.31	VLITE
2021 Jan 0.8	5998.6	21.52 ± 4.30	VLITE

^a Includes additional 5% flux error as the observation was dynamic range limited.

^b Includes additional 10% flux error as this is a quick-look observation from VLASS.

Within the SSA model, we consider emission produced at a certain epoch t since explosion (i.e., $t = 0$ at the

time of the explosion of the SN, t_e) from a thin shell of radiating electrons of radius r , and thickness r/η . The electrons are accelerated to a power-law distribution of Lorentz factors $N(\gamma) \propto \gamma^{-p}$, above a minimum Lorentz factor γ_m . The temporal evolution of the radius of the shell, of the magnetic field, and of the minimum Lorentz factor are assumed to follow the relations:

$$r(t) = r_0 \left(\frac{t}{t_0} \right)^{\alpha_r}, \quad (1)$$

$$B(t) = B_0 \left(\frac{t}{t_0} \right)^{\alpha_B}, \quad (2)$$

$$\gamma_m(t) = \gamma_{m,0} \left(\frac{t}{t_0} \right)^{\alpha_\gamma}, \quad (3)$$

where t_0 is an arbitrary reference epoch, t is the epoch since explosion t_e , and r_0 , B_0 , $\gamma_{m,0}$ are the values of the shell radius, magnetic field, and electron minimum Lorentz factor at this reference epoch, respectively. Also, the density profile of the radiating electrons within the shocked CSM is assumed to be $n_e \propto r^{-s}$. Assuming also equipartition, i.e. $\epsilon_e = \epsilon_B$ for the fraction of energy going into relativistic electrons and magnetic field respectively (see e.g., [Wellons et al. 2012](#)), one has:

$$\alpha_B = \frac{(2-s)}{2} \alpha_r - 1 \quad \text{and} \quad \alpha_\gamma = 2(\alpha_r - 1). \quad (4)$$

The flux density at a certain epoch t and frequency ν is given by:

$$f_\nu = C_f \left(\frac{t}{t_0} \right)^{(4\alpha_r - \alpha_B)/2} \left[1 - e^{-\tau_\nu^\xi(t)} \right]^{1/\xi} \nu^{5/2} F_3(x) F_2^{-1}(x), \quad (5)$$

where the optical depth $\tau_\nu(t)$ reads:

$$\tau_\nu = C_\tau \left(\frac{t}{t_0} \right)^{(p-2)\alpha_\gamma + (3+p/2)\alpha_B + \alpha_r} \nu^{-(p+4)/2} F_2(x), \quad (6)$$

and where $\xi \in [0, 1]$ controls the sharpness of the spectral break between optically thin and thick regimes. In the above equations, F_2 and F_3 are Bessel functions of $x = 2/3(\nu/\nu_m)$ with ν_m the critical synchrotron frequency of electrons with Lorentz factor equal to γ_m . This frequency, ν_m , evolves with time as:

$$\nu_m = \nu_{m,0} \left(\frac{t}{t_0} \right)^{(10\alpha_r - s\alpha_r - 10)/2}, \quad (7)$$

where:

$$\nu_{m,0} = \gamma_{m,0}^2 \frac{eB}{2\pi m_e c}. \quad (8)$$

The normalization constants for the flux density and optical depth, C_f and C_τ , are themselves functions of B_0 , $\nu_{m,0}$, r_0 (see Equations (A13)-(A14) in [Soderberg et al. 2005](#)):

$$C_f = \frac{2\pi m_e}{2+p} \left(\frac{r_0}{d} \right)^2 \left(\frac{2\pi m_e c}{eB_0} \right)^{1/2}, \quad (9)$$

$$C_\tau = \frac{(p+2)(p-2)\gamma_{m,0}^{(p-1)}}{4\pi\eta} \frac{B_0^2}{8\pi m_e^3 c^4 \gamma_{m,0}} \left(\frac{eB_0}{2\pi m_e c} \right)^{p/2}, \quad (10)$$

where d is the distance to the source.

At high frequencies, the observed spectral flux density needs to be corrected for the effects of synchrotron cooling, which occurs at frequencies above the cooling frequency (ν_c), defined as:

$$\nu_c = \frac{18\pi m_e c e}{t^2 \sigma_T^2 B^3}. \quad (11)$$

Overall, the resulting spectral shape and temporal evolution of the flux density from Equation (5), corrected for the effects of synchrotron cooling, can be approximated as:

$$f_\nu \propto \begin{cases} \nu^2 t^{2\alpha_r + \alpha_\gamma} & \nu < \nu_m, \\ \nu^{1/3} t^{(4\alpha_r - \alpha_B)/2} & \nu_m < \nu < \nu_a, \\ \nu^{-(p-1)/2} t^{[4\alpha_r - \alpha_B + (4+p)\alpha_{\nu_a}]/2} & \nu_a < \nu < \nu_c, \\ \nu^{-p/2} t^{[2\alpha_r + (1-3p)\alpha_B + (2+p/2)\alpha_{\nu_a} - 2p + 1]} & \nu > \nu_c \end{cases} \quad (12)$$

where $\nu_m \ll \nu_a$, typically a good assumption at late times, and:

$$\nu_a = \nu_{a,0} \left(\frac{t}{t_0} \right)^{[2(p-2)\alpha_\gamma + 2(3+p/2)\alpha_B + 2\alpha_r]/(p+4)} = \nu_{a,0} \left(\frac{t}{t_0} \right)^{\alpha_{\nu_a}}. \quad (13)$$

Note that in the above Equation, $\nu_{a,0}$ can be calculated using the condition $\tau_{\nu_{a,0}}(t_0) = 1$.

Based on the above considerations, for a given t_e , via comparison with flux density observations at different times and frequencies, one can determine the set of parameters (B_0 , α_r , p , $\nu_{m,0}$, r_0 , s , ξ). These, in turn, constrain the physics of the emitting shell and the properties of the CSM. Specifically, one can derive constraints (see e.g., [Soderberg et al. 2006](#)) on the ejecta energy,

$$E = \frac{4\pi}{\eta} r_0^3 \frac{B_0^2}{8\pi\epsilon_e} \left(\frac{t}{t_0} \right)^{(5\alpha_r - s\alpha_r - 2)} \quad (14)$$

electron density,

$$n_e = \frac{(p-2)}{(p-1)} \frac{B_0^2}{8\pi m_e c^2 \gamma_{m,0}} \left(\frac{r}{r_0} \right)^{-s}, \quad (15)$$

and the mass loss rate,

$$\dot{M} = \frac{8\pi n_{e,0} m_p r_0^2 v_w (p-2)}{\eta (p-1)} \frac{B_0^2}{8\pi m_e c^2 \gamma_{m,0}} \left(\frac{r}{r_0} \right)^{(2-s)}. \quad (16)$$

In the above Equation, v_w is the wind velocity and $n_{e,0}$ is the value of n_e at $t = t_0$. Hereafter, we take $v_w = 1000 \text{ km s}^{-1}$, the typical value for Galactic Wolf-Rayet stars (see [Wellons et al. 2012](#)).

4. RESULTS

Using all detections reported in Table 1, we perform a χ^2 fit of the SN 2004dk radio observations within the

SSA model described in the previous Section. For all fits, we set $t_0 = 10$ days from the explosion time t_e and, following Wellons et al. (2012), $\eta = 4$. Table 2 shows the best fit results obtained for various scenarios. The orange fit (and corresponding orange lines in Figures 2 and 3) considers only data obtained within the first ~ 100 days from the SN 2004dk explosion, so as to exclude the radio re-brightening phase. For this fit, following the “standard” fit by Wellons et al. (2012), we fix $\alpha_r = 0.9$, $p = 3.0$, $s = 2.0$, and $\xi = 1.0$. We further set $\nu_{m,0} = 0.02$ GHz (Soderberg et al. 2006) and allow B_0 and r_0 to vary. The obtained best fit values for B_0 and r_0 agree with those by Wellons et al. (2012). This best fit yields a $\chi^2/dof \approx 174/18$.

TABLE 2 The best fit results for SN 2004dk within the SSA model. See text for discussion.

Parameters	Orange fit	Red fit	Blue fit
B_0 (G)	1.06	0.02	3.27
α_r	0.9 ^f	0.9 ^f	0.9 ^f
p	3.0 ^f	3.0 ^f	3.0 ^f
$\nu_{m,0}$ (GHz)	0.02 ^f	0.02 ^f	0.02 ^f
r_0 ($\times 10^{15}$ cm)	5.0	5.0 ^f	5.0 ^f
s	2.0 ^f	0.0	2.0 ^f
t_e (JD)	2453217.7 ^f	2453217.7 ^f	2453217.7 ^f
ξ	1.0 ^f	0.2	1.0
χ^2/dof	173.80/18	101.06/11	495.44/12
$\gamma_{m,0}$	2.6	20.1	1.5
E_0 (erg)	1.8×10^{47}	4.9×10^{43}	1.7×10^{48}
v_0 (c)	0.17	0.17	0.17
$n_{e,0}$ (cm^{-3})	1.0×10^4	3.8×10^{-1}	1.8×10^5
\dot{M}_0 (M_\odot/yr)	4.4×10^{-6}	1.6×10^{-10}	7.4×10^{-5}

^f fixed parameter

Next, we perform an independent analysis of the late-time ($t \gtrsim 1000$ d since explosion) radio observations of SN 2004dk within the SSA model. All the fits assume a smooth radial evolution of the SN 2004dk ejecta with $\alpha_r = 0.9$ and $r_0 = 5.0 \times 10^{15}$ cm (as derived from the fit of the early-time data). For the red fit (and corresponding red lines in Figures 2 and 3) we fix $\nu_{m,0} = 0.02$ GHz, and $p = 3.0$, and vary B_0 and s and ξ . The best fit result yields $s \approx 0$ and a $\chi^2/dof \approx 101/11$. For comparison, we also report a blue fit (and corresponding blue lines in Figures 2 and 3) where we set $s = 2$ (standard case of a smooth CSM shaped by a constant mass-loss rate from the progenitor). We see in Figure 2 that the blue curve does not fit the data well ($\chi^2/dof \approx 495/12$).

5. DISCUSSION AND CONCLUSION

From the outcome of the fits reported in the previous Section, it is evident that the standard $s = 2$ (constant mass-loss rate) and $p = 3$ scenario of the SSA model for radio SNe fits the SN 2004dk radio data well at early times ($t \lesssim 100$ days since explosion, orange fit in Figure 2) and agrees with the fit obtained by Wellons et al. (2012). However, interpreting the SN 2004dk late-time radio re-brightening within the SSA scenario requires a

modified CSM profile which approaches the $s = 0$ case of a constant density ISM (compare the blue fit with the red one).

Changes in the mass-loss rate profile at late times have been observed in other SNe with peculiar and variable radio light curves (e.g., Montes et al. 1998; Wellons et al. 2012; Corsi et al. 2014; Palliyaguru et al. 2019) and can be attributed to a significant evolution in the mass-loss history of the SN progenitor in the years before explosion, perhaps related to precursor eruptions to the main SN event. In Figure 3, we show the evolution of the mass-loss rate with radius (bottom right panel) for the late-time best fit models of SN 2004dk radio light curves, compared to that derived from the early-time data (orange).

It is particularly interesting that the fit providing the best χ^2/dof pushes the parameter s to $s = 0$, so that a constant ISM density profile seems to be favored over a stellar wind one (see Chevalier 1982, for a discussion of the $s = 0$ case). To better understand the reasons behind this result, the following considerations are useful. As shown in the bottom-right panel in Figure 2, our observing radio frequencies ν (light blue patch) are such that, for all best fit models considered here, $\nu_m < \nu_a < \nu < \nu_c$. Thus, from Equation (12), we expect the flux to scale as:

$$f_\nu \propto t^{\frac{1}{4}(6\alpha_r - 5s\alpha_r + 10p\alpha_r - 10p - sp\alpha_r + 6)}. \quad (17)$$

As is evident from the above Equation, when $s = 0$ (and for $\alpha_r = 0.9$ and $p = 3$), f_ν increases with time in this frequency regime, while for $s = 2$ (blue fit in Figure 2) the flux decrease with time, thus making it hard to fit a re-brightening behavior such as the one observed in SN 2004dk (see Figure 2).

From Equations (16)-(17), when $s \neq 2$ we can further derive the following scaling of the observed flux with the mass-loss rate:

$$f_\nu \propto \left(\frac{\dot{M}}{v_w} \right)^{\frac{[\alpha_r(6-5s+10p-sp) - 10p + 6]}{(4\alpha_r(2-s))}}. \quad (18)$$

For $\alpha_r = 0.9$, $p = 3$, and $s = 0$, one gets:

$$f_\nu \propto \left(\frac{\dot{M}}{v_w} \right)^{+1.2} \quad (19)$$

which shows how an increase in mass-loss rate corresponds to a re-brightening of the observed flux (see Figure 3 for the radial evolution of the mass-loss rate, and Figure 2 for the temporal evolution of the flux density).

Finally, we can compare our results with those reported in Mauerhan et al. (2018), where the velocity measurements from late-time observations of the H α profiles yielded $v_w \approx 400$ km s $^{-1}$. Assuming this to be the speed of an H-rich CSM outflow from the progenitor system, we find that the H-rich CSM was ejected ≈ 400 years before explosion (since the SN shock meets this CSM outflow at a radius of $\approx 5 \times 10^{17}$ cm). This estimate closely agrees with the estimate of ≈ 320 years found by Mauerhan et al. (2018), which suggests a “superwind”, related to pulsations of the partially ionised H envelope during the red supergiant phase (Heger et al. 1997). Computational studies of such a mechanism show that winds can cause episodic mass loss from the star, all in a timescale

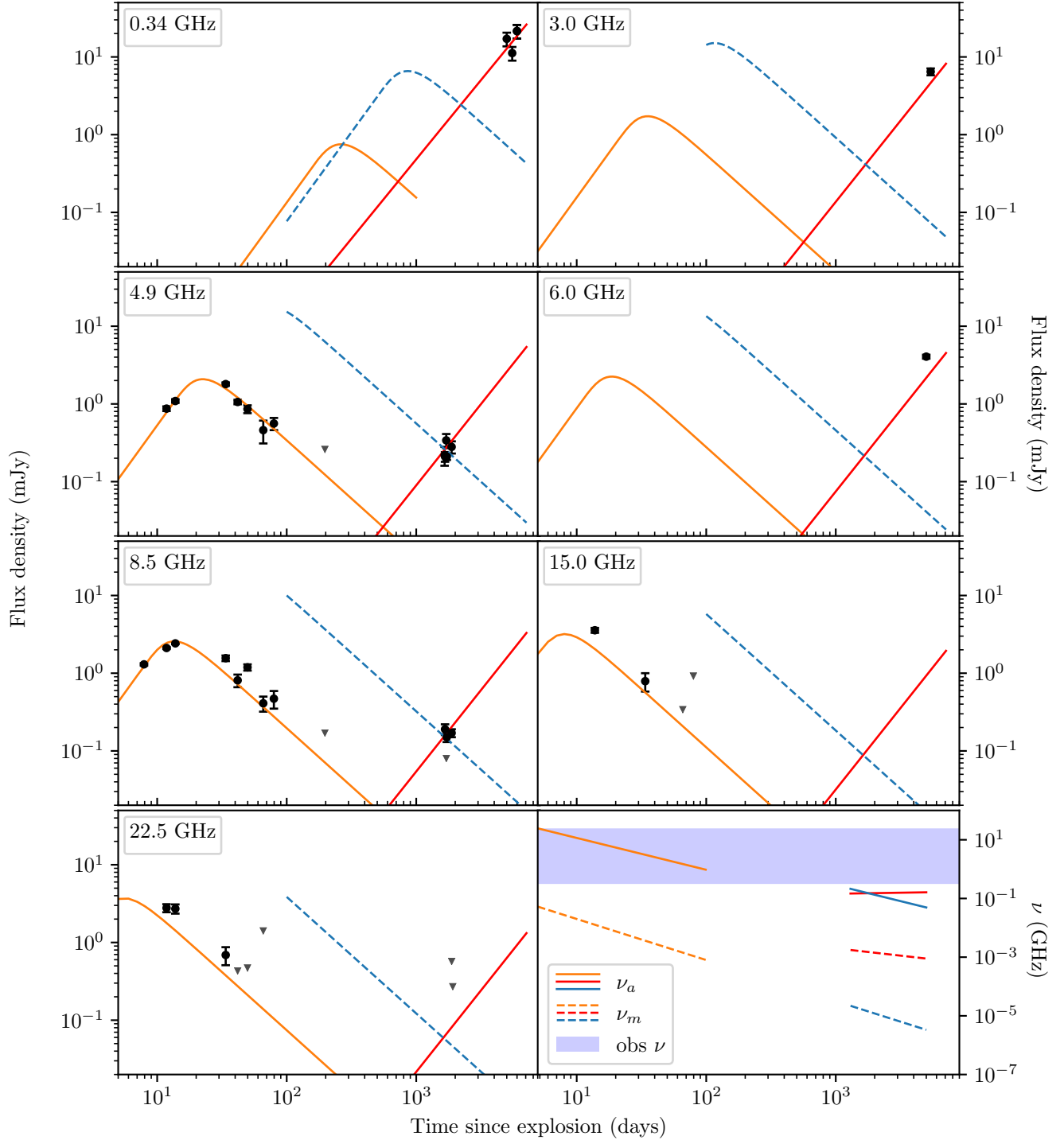


FIG. 2.— The radio light curves of SN 2004dk (data points) with the best fit models (lines; see also Table 2). Upper limits are shown as downward pointing triangles and are not included in the fits. The orange curve agrees with the fit obtained by Wellons et al. (2012). Curves at later times (red and blue) are fits derived assuming a smooth radial evolution of the SN ejecta. The last panel of the plot shows the temporal evolution of ν_a (solid lines) and ν_m (dashed lines) and the color code is the same as that of the light curves. The extent of the light blue patch covers the observation frequencies from the lowest 340 MHz to the highest 22.5 GHz.

of $\lesssim 10^3$ years before the explosion (Yoon & Cantiello 2010).

In conclusion, the VLITE observations reported in this paper, combined with previously collected VLA data, favor an interpretation of SN 2004dk as a strongly CSM-interacting radio SN going through an environment shaped by the progenitor wind at first, and then followed by an ISM-like profile. However, our conclusions are limited by the simplifications inherent in the spherically symmetric SSA model adopted here. Continued VLA/VLITE observations will be able to further test this hypothesis (or

else spur a more complex theoretical modeling of this peculiar radio SN light curve).

A.B. and A.C. acknowledges support from the National Science Foundation CAREER Award #1455090. The National Radio Astronomy Observatory is a facility of the National Science Foundation operated under cooperative agreement by Associated Universities, Inc. Basic research in radio astronomy at the Naval Research Laboratory is funded through 6.1 Base funding.

REFERENCES

- Begelman, M. C., & Sarazin, C. L. 1986, *ApJ*, 302, L59
 Chevalier, R. A. 1982, *ApJ*, 258, 790
 Chevalier, R. A. 1998, *ApJ*, 499, 810
 Chevalier, R. A., & Fransson, C. 2006, *ApJ*, 651, 381
 Clarke, T. E., Kassim, N. E., Briskeen, W., Helmboldt, J., Peters, W., Ray, P. S., Polisenky, E., & Giacintucci, S. 2016, in *Society of Photo-Optical Instrumentation Engineers (SPIE) Conference Series*, Vol. 9906, *Ground-based and Airborne Telescopes VI*, 99065B
 Clarke, T. E., et al. 2011, in *General Assembly and Scientific Symposium*, E5
 Corsi, A., et al. 2014, *ApJ*, 782, 42
 Cotton, W. D. 2008, *PASP*, 120, 439
 Deller, A. T., Tingay, S. J., Bailes, M., & West, C. 2007, *PASP*, 119, 318
 Filippenko, A. V. 1997, *ARA&A*, 35, 309
 Filippenko, A. V., Ganeshalingam, M., Serduke, F. J. D., & Hoffman, J. L. 2004, *IAU Circ.*, 8404, 1
 Flewelling, H. A., et al. 2020, *ApJS*, 251, 7
 Graham, J., & Li, W. 2004a, *Central Bureau Electronic Telegrams*, 75, 1
 Graham, J., & Li, W. 2004b, *IAU Circ.*, 8377, 2
 Heger, A., Jeannin, L., Langer, N., & Baraffe, I. 1997, *A&A*, 327, 224
 Ho, A. Y. Q., et al. 2019, *ApJ*, 887, 169
 Joye, W. A., & Mandel, E. 2003, in *Astronomical Society of the Pacific Conference Series*, Vol. 295, *Astronomical Data Analysis Software and Systems XII*, ed. H. E. Payne, R. I. Jedrzejewski, & R. N. Hook, 489
 Lacy, M., et al. 2020, *PASP*, 132, 035001
 Margutti, R., et al. 2017, *ApJ*, 835, 140
 Mauerhan, J. C., Filippenko, A. V., Zheng, W., Brink, T. G., Graham, M. L., Shivvers, I., & Clubb, K. I. 2018, *MNRAS*, 478, 5050
 McMullin, J. P., Waters, B., Schiebel, D., Young, W., & Golap, K. 2007, in *Astronomical Society of the Pacific Conference Series*, Vol. 376, *Astronomical Data Analysis Software and Systems XVI*, ed. R. A. Shaw, F. Hill, & D. J. Bell, 127
 Mohan, N., & Rafferty, D. 2015, *PyBDSF: Python Blob Detection and Source Finder*
 Montes, M. J., Van Dyk, S. D., Weiler, K. W., Sramek, R. A., & Panagia, N. 1998, *ApJ*, 506, 874
 Ofek, E. O., Frail, D. A., Breslauer, B., Kulkarni, S. R., Chandra, P., Gal-Yam, A., Kasliwal, M. M., & Gehrels, N. 2011, *ApJ*, 740, 65
 Palliyaguru, N., & Corsi, A. 2019, in *American Astronomical Society Meeting Abstracts*, Vol. 233, *American Astronomical Society Meeting Abstracts #233*, 258.09
 Palliyaguru, N. T., et al. 2019, *ApJ*, 872, 201
 Perley, R. A., & Butler, B. J. 2017, *ApJS*, 230, 7
 Piro, A. L., & Nakar, E. 2013, *ApJ*, 769, 67
 Podsiadlowski, P., Joss, P. C., & Hsu, J. J. L. 1992, *ApJ*, 391, 246
 Polisenky, E., et al. 2016, *ApJ*, 832, 60
 Polisenky, E., Richards, E., Clarke, T., Peters, W., & Kassim, N. 2019, in *Astronomical Society of the Pacific Conference Series*, Vol. 523, *Astronomical Data Analysis Software and Systems XXVII*, ed. P. J. Teuben, M. W. Pound, B. A. Thomas, & E. M. Warner, 4 adsurl = <https://ui.adsabs.harvard.edu/abs/2019ASPC..523..441P>, adsnote = Provided by the SAO/NASA Astrophysics Data System
 Pooley, D. 2007, in *American Institute of Physics Conference Series*, Vol. 937, *Supernova 1987A: 20 Years After: Supernovae and Gamma-Ray Bursters*, ed. S. Immler, K. Weiler, & R. McCray, 381
 Pooley, D., et al. 2019, *ApJ*, 883, 120
 Rivera Sandoval, L. E., Maccarone, T. J., Corsi, A., Brown, P. J., Pooley, D., & Wheeler, J. C. 2018, *MNRAS*, 480, L146
 Smith, N., Li, W., Filippenko, A. V., & Chornock, R. 2011, *MNRAS*, 412, 1522
 Soderberg, A. M., Chevalier, R. A., Kulkarni, S. R., & Frail, D. A. 2006, *ApJ*, 651, 1005
 Soderberg, A. M., Kulkarni, S. R., Berger, E., Chevalier, R. A., Frail, D. A., Fox, D. B., & Walker, R. C. 2005, *ApJ*, 621, 908
 Stockdale, C. J., et al. 2009, *Central Bureau Electronic Telegrams*, 1714, 1
 van Moorsel, G., Kembell, A., & Greisen, E. 1996, in *Astronomical Society of the Pacific Conference Series*, Vol. 101, *Astronomical Data Analysis Software and Systems V*, ed. G. H. Jacoby & J. Barnes, 37
 Vinko, J., et al. 2017, *ApJ*, 837, 62
 Weiler, K. W., Panagia, N., & Sramek, R. A. 1990, *ApJ*, 364, 611
 Wellons, S., Soderberg, A. M., & Chevalier, R. A. 2012, *ApJ*, 752, 17
 Wheeler, J. C., & Levreault, R. 1985, *ApJ*, 294, L17
 Woosley, S. E., Langer, N., & Weaver, T. A. 1995, *ApJ*, 448, 315
 Yoon, S.-C., & Cantiello, M. 2010, *ApJ*, 717, L62

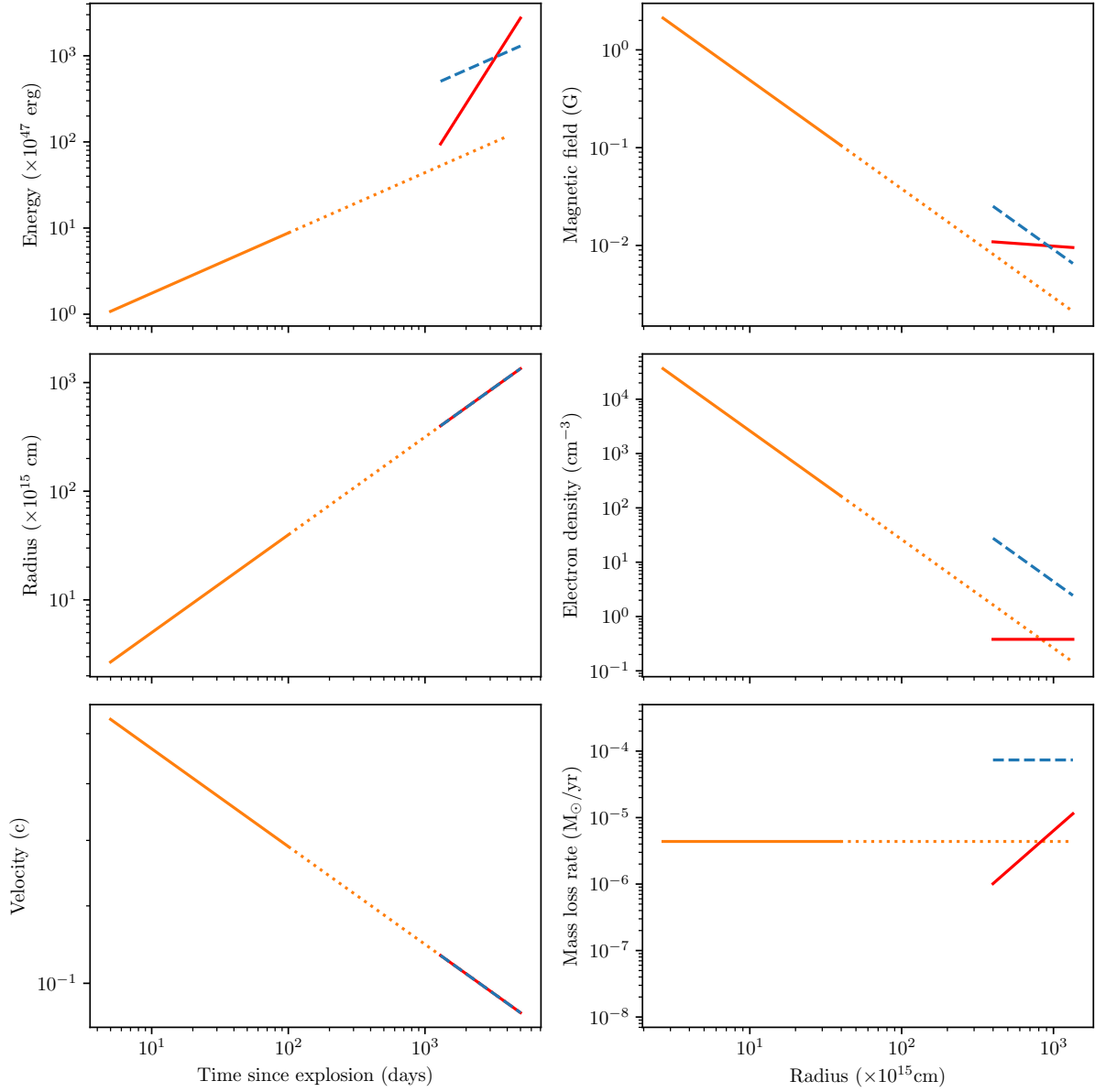


FIG. 3.— Plot of physical parameters for various fits using the same colors as the light curve plot (Figure 2). The panels on the left show the temporal evolution of the shocked shell properties, while the panels on the right show the radial evolution of the ambient medium and magnetic field. See text for discussion.